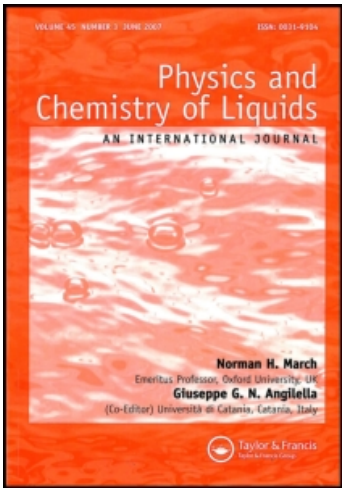

Physics and Chemistry of Liquids
Publication details, including instructions for authors and subscription information:
http://www.informaworld.com/smpp/title~content=t713646857

Molecular and Brownian Dynamics Simulations of Self-Diffusion in Inverse Power Fluids

D. M. Heyes[a]; A. C. Brańka[ab]
[a] Department of Chemistry, University of Surrey, Guildford [b] Institute of Molecular Physics, Polish Academy of Sciences, Poland

To cite this Article Heyes, D. M. and Brańka, A. C.(1994) 'Molecular and Brownian Dynamics Simulations of Self-Diffusion in Inverse Power Fluids', Physics and Chemistry of Liquids, 28: 2, 95 — 115
To link to this Article: DOI: 10.1080/00319109408029546
URL: http://dx.doi.org/10.1080/00319109408029546

Phys. Chem. Liq., 1994, Vol. 28, pp. 95–115
Reprints available directly from the publisher
Photocopying permitted by license only

MOLECULAR AND BROWNIAN DYNAMICS SIMULATIONS OF SELF-DIFFUSION IN INVERSE POWER FLUIDS

D. M. HEYES and A. C. BRAŃKA*

Department of Chemistry, University of Surrey, Guildford, GU2 5XH

(Received 17 January 1994)

We compare the structural, thermodynamic and dynamical behaviour of a model colloidal system with that of the equivalent atomic system using the simulation techniques of brownian dynamics and molecular dynamics. In the process we establish the important role made by solvent mediated many-body hydrodynamics on colloidal single particle motion on "short" and "long" time scales. The short and long-time self-diffusion coefficients of model stabilised colloidal particles were calculated at solids volume fractions up to 0.527 using a hydrodynamics-free Brownian Dynámics, *BD* technique with model colloidal particles interacting through a r^{-36} repulsive pair potential. We have improved the simulation technique to follow the self-diffusion process over several molecular diameters, required for the evaluation of the long-time diffusion coefficient. The simulation long-time diffusion coefficient follows closely the behaviour of the experimental *short*-time diffusion coefficient for volume fractions below *ca.* 0.4.

KEY WORDS: Colloidal particles, many-body hydrodynamics.

1 INTRODUCTION

The self-diffusion behaviour of colloidal particles can be interpreted in the light of essentially two key time-scales. As a consequence of the large colloidal particle mass, its velocity fluctuates on a "Brownian time scale", $\tau_B = m/\xi$, where m, is the Brownian particle's mass and ξ, is the Stokes friction coefficient (for stick boundary conditions, $\xi = 3\pi\eta_s\sigma$, where η_s, is the solvent viscosity and σ is the diameter of the Brownian particle). The timescale, τ_B, is many orders of magnitude smaller than the time it takes the particle to move a distance of order its diameter which we denote by, $\tau_r \sim \sigma^2/D_0$. D_0 is the self-diffusion coefficient of the colloidal particle at infinite dilution, which is related to the friction coefficient by, $D_0 = k_BT/\xi$ where T is the temperature. For time scales increasing from τ_B, self-diffusion of the colloidal particle is dominated by a range of coupled processes which include the random collisions from the solvent molecules, the solvent viscosity, the medium-mediated hydrodynamic interactions between the colloidal particles, temperature and the potential field established by the other colloidal particles at each time. The self-diffusion of the colloidal particle is influenced by all of these factors. At very short times a colloidal particle diffuses in an approximately static configuration of surrounding molecules. This is called the "short time" regime. In the time, t range, $\tau_r \gg t \gg \tau_B$ the self-diffusion coefficient is essentially

* *Permanent address*: Institute of Molecular Physics, Polish Academy of Sciences, Smoluchowskiego 17/19, 60–179, Poland.

constant and is called the short time diffusion coefficient, D^S. At longer times, after a particle has diffused a distance of order its diameter, the diffusion process has been slowed down by the interaction of the particle with its cage of particles. This quantity is less amenable to a purely analytical description because changes in the neighbouring particles' positions during the translational motion need to be taken into account. The hindered passage of the particle through its cage of surrounding particles slows down its rate of progress, resulting in the diffusion coefficient in this "long-time" regime falling below the value of D^S. As $t \gg \tau_r$ the diffusion coefficient tends to a constant value, which is called the "long-time" self-diffusion coefficient D^L. Both self-diffusion coefficients can also be obtained from the ratio of the average velocity of a tagged particle subjected to an external force [1]. The short time diffusion coefficient has been measured by multiple light scattering, [2] while the long time diffusion coefficient is amenable to a wider range of techniques including florescence recovery [3] and photon correlation spectroscopy [4, 5].

Both D^S and D^L depend on solids volume fraction. The difference between D^S and D^L is some measure of to what extent a colloidal particle is retarded by coupled solvent-mediated forces and particle migration at long times. In the limit of the volume fraction $\phi \to 0$,

$$D^L = D_0(1 - a\phi) \quad t \gg \tau_r, \tag{1}$$

and $\phi = \pi N\sigma^3/6V$. There are a range of values for the constant a in the literature; analytic values of a depend on the level of the dynamical approximation, ranging between $-0.08 < a < -2.625$, for example [6]. There have been experimental measurements of the volume fraction dependence of D^S and D^L over the whole liquid range [2, 4]. $D^L/D_0 < 0.1$ at the volume fraction at which crystallisation takes place [7].

It is interesting to compare the dynamical behaviour of the model colloidal liquids and their molecular fluid counterparts. Both types of fluid can be to a certain extent represented by an equivalent hard-sphere fluid, on assignment of an effective hard-sphere diameter, σ to the real particle [11, 12]. A knowledge of the density dependence of the transport coefficients of the hard-sphere fluid is often required. The density dependence of the self-diffusion coefficient of the hard-sphere fluid is now well-known, with several analytic fits in the literature. For N hard-spheres in volume V, we define a reduced number density, $\rho = N\sigma^3/V$. A fit to simulation data given by Speedy [8] is,

$$D = D_{00}\left(1 - \left(\frac{\rho}{1.09}\right)\right)(1 + \rho^2(0.4 - 0.83\rho^2)). \tag{2}$$

Erpenbeck and Wood have been fitted their MD hard-sphere simulation data to the expression,

$$D = D_E(1 + a_1\rho + a_2\rho^2 + a_3\rho^3), \tag{3}$$

where $a_1 = 0.038208154$, $a_2 = 3.182808$ and $a_3 = -3.868771766$. Both Eq. (2) and Eq. (3) include a reference self-diffusion coefficient. The diffusion coefficient for an ideal hard sphere gas, D_{00}, is determined from kinetic theory to be,

$$D_{00} = 3(k_B\, T/\pi m)^{1/2}/8\rho\sigma^2, \tag{4}$$

and D_E is the Enskog theory extension of these basic assumptions to finite density,

$$D_E = 1.01896\, D_{00}/g(\sigma), \tag{5}$$

where $g(\sigma)$ is the value of the pair radial distribution function at the contact of the spheres.

In the context of colloidal liquids, Eq. (2) and Eq. (3) are conceptually unsatisfactory, because they use a reference self-diffusion coefficient which is based on the kinetic theory of gases in the limit of zero density, D_{00} or alternatively, its finite density extension, D_E. There is no reason to expect the ideal gas to be pertinent to the colloidal state. Nevertheless, the behaviour of the "molecular" hard-sphere fluid at finite densities should, in some sense, still be relevant to colloids because, as volume fraction increases, excluded volume effects should act in both the molecular (i.e., hard-sphere) and colloidal liquids to slow down self-diffusion.

An alternative representation of hard-sphere molecular dynamics data, developed from the pioneering work of Hildebrand [27], by Dymond [28], and the others, e.g., [29], has similarities with the behaviour of colloidal liquid (see Figure 11). Significantly, it does not use the kinetic theory of gases as its basis,

$$D/D_{00} = 1.271\rho(\rho_0/\rho - 1.384)/\rho_0, \tag{6}$$

where $\rho_0 = 2^{1/2}$ is the close-packed density of the f.c.c. crystal. This formula is an empirical fit to simulation data which emphasises the dominance of excluded volume effects at high density. The coefficient, D_{00} does appear in Eq. (6) to confer a realistic temperature dependence to D but otherwise makes no attempt to go over to the low density limit correctly. The formula in Eq. (6) has a low density limit that is not that of the ideal gas. Equation (6) is better expressed for the present work in the volume fraction form,

$$D/D_{00} = 1.271 - 2.37557\phi. \tag{7}$$

Equation (7) has the limit $D \to 0$ at a volume fraction of 0.54, which is equal to the solid density at melting for a hard-sphere system. We will show that similar excluded volume effects are present in the model colloidal liquids which result in a density dependence to the long-time diffusion coefficient of the same generic form as in Eq. (7) applicable to atomic fluids.

We use the simulation techniques of molecular dynamics and brownian dynamics to investigate the single particle dynamical behaviour of particles in model molecular and colloidal systems, especially that relevant to the self-diffusion coefficients. The model particles interact with the same potential but undergo different equations of motion. This enables us to establish more clearly the similarities and differences caused by the different equations of motion. We choose an inverse power potential, rather than a Yukawa potential because it has more convenient scaling properties, and is formally more closely related to the hard-sphere reference fluid.

We compare the calculated self-diffusion coefficients with experimental data on colloidal liquids and those from other brownian dynamics simulations. In the next section we outline the theoretical background to our model and its analysis.

2 THEORETICAL BACKGROUND

2.1 *Equations of motion*

The colloidal liquid consists of interactions and processes taking place over a wide range of time and distance scales. As a result, for mathematical and computational convenience the colloidal liquid is modelled as a suspension of large and massive macroparticles or "Brownian" particles in a continuum Newtonian fluid medium. In this approach the particles interact through both interparticle colloidal forces and hydrodynamic forces mediated by the solvent. In addition, the solvent provides for each macroparticle a fluctuating thermal force which produces the well-known phenomenon of Brownian motion. The interparticle interactions are in many respects similar to those of simple liquids or gases and often can be represented quite well by a sum of interactions solely between pairs of particles. The hydrodynamic interactions are characteristic of the colloidal liquid (medium and particles), which are less tractable and the pair-wise additive approximation is not good.

Because of the approximate treatment of the solvent, the basic equations of motion for N-interacting Brownian particles are not Newton's equations but ($3N$ coupled) Langevin equations, with an *assumed* extension to include interacting particles, [14]

$$\dot{\underline{p}} = -\xi \underline{p} + \underline{R} + \underline{F}, \tag{8}$$

where $\underline{p}$ is the momentum of the brownian particle, $\underline{R}$ is the brownian force on the colloidal particle, which is represented by a normally distributed random number. $\underline{F}$ is the systematic or direct force between the colloidal particles (including any external force). The mass of the brownian particles is assumed to be many orders of magnitude greater than that of the solvent molecules.

The time average of a dynamical quantity obtained from a phase space trajectory generated by the Langevin equations is equivalent to the phase space distribution average obtained from the Fokker–Planck equation. The stationary solution of the Fokker–Planck equation is the canonical distribution function. By virtue of this fact, static properties of the Brownian particle system are not influenced by hydrodynamic interactions and are the same as calculated from canonical MD or MC simulations for a system of particles with the same interparticle interactions. It should be stressed, however, that presence of a solvent will modify quite dramatically the dynamics of the particles. Consequently the dynamical properties of a Brownian particle system and its MD conterpart are quite different (The reason for that is that the time evolution in these two systems is determined by the different dynamic operators [30]).

For most treatments of the dynamics of interacting Brownian particles, only the configurational evolution, which proceeds on a timescale much greater than τ_B, is relevant. In this case the Langevin equations reduce to the "position Langevin equation". The associated equation of motion for the configurational distribution function is the Smoluchowski equation. The Langevin/Smoluchowski position level of equations, like the momentum Langevin/Fokker–Planck level equations, produces canonical averages which, in the case of static quantities, are independent of hydrodynamic interactions and are equal to the MD or MC averages. This independence

of the nature of the simulation method (*MD*, *MC*, and *BD*) for static properties provides a good consistency test of the simulations.

Our Brownian dynamics simulations are based on the position Langevin equation. If many-body hydrodynamic interactions are neglected this equation leads to the following position updating algorithm for the particle positions in time-steps, h, [31].

$$\underline{r}_i(t+h) = \underline{r}_i(t) + \frac{D_0}{k_B T}\underline{F}_i(t)h + \underline{\Delta r}_i(t,h) \tag{9}$$

where $i = 1, \ldots, N$ are the particle labels, $\underline{F}$ is the systematic or direct forces between the colloidal particles (including any external force) and $\underline{\Delta r}$ is the random displacement sampled from a gaussian distribution of zero mean and variance $\langle \Delta r^2 \rangle = 6D_0 h$.

The main impediment to implementation of the *BD* method with hydrodynamic interactions at the high concentrations studied here is that a simple closed form for them is not available. The hydrodynamic interaction, represented by a mobility tensor is well-known for an isolated pair of spheres in an incompressible fluid. Although the formulae for three and four body terms (essential at volume fractions in excess of 0.1) have been derived, [15] their incorporation in a simulation is prohibitively expensive and formally higher order terms should also be included. In an important paper van Megen *et al.* showed that the three particle contribution to the self-diffusion coefficients is typically of the same order of magnitude as the two particle term, so the rate of convergence of the n-body expansion is extremely slow [16, 17]. As yet there is no concensus on implementation of this aspect of colloidal dynamics. A number of models which attempt to include many-body hydrodynamics in an *ad-hoc* manner using a diversity of prescriptions are in the literature [18, 19]. One could argue that even if the full N-body hydrodynamics were included in the model that the full picture for dense suspensions would not be arrived at, as excluded solvent effects (when two colloidal particles are close to $r = \sigma$ apart) should also be taken into account. For these reasons we have decided here to omit many-body hydrodynamics to discover how a basic model for colloidal dynamics (which is still frequently used) distinguishes itself from that of particles interacting through the same pair potential but subject to Newton's equations of motion. We especially focus attention on the self-diffusion behaviour, to establish the BD model's strengths and limitations by comparing its predictions with recent experimental data.

2.2 *Self-diffusion coefficients*

The diffusion coefficient of the Brownian particles is not well-defined at short times and it is assumed to be time dependent. (Only D^L is unambiguous at $t \to \infty$.) The time dependent self-diffusion coefficient can be defined as being proportional to the "local' slope of the mean square displacement with time, i.e.,

$$D(t) = \frac{1}{6}\frac{d\langle \Delta r(t)^2 \rangle}{dt}, \tag{10}$$

or alternatively,

$$D(t) = \frac{1}{6t}\langle \Delta r(t)^2 \rangle. \tag{11}$$

In the long-time diffusion limit both (10) and (11) give the same answer [21]. For all fluids at extremely short times $\sim 10^{-12}$ s, the initial increase of the mean-square displacement is quadratic in time, as each particle is in "free flight". Then the mean square displacements are given by,

$$\langle \Delta \underline{r}(t)^2 \rangle = 3k_B T t^2/m. \tag{12}$$

In the colloidal liquid, one has at infinite dilution, another time-scale of τ_B which marks the onset of diffusive motion of the colloidal particle through the solvent [30]. At infinite dilution an explicit expression for $D(t)$ can be obtained from the Langevin equation which illustrates the crossover from *very* short times where Newton's equations of motion need to be considered, to the short-time regime where the motion can be described as "diffusive" [10].

$$\langle \Delta \underline{r}(t)^2 \rangle = 6D_0(t - \tau_B(1 - \exp(-t/\tau_B)) \tag{13}$$

For $t \ll \tau_B$, (13) reduces to (12). For $t \gg \tau_B$ we enter the time domain of diffusive motion,

$$\langle \Delta \underline{r}(t)^2 \rangle = 6D_0 t. \tag{14}$$

In the position Langevin equations of motion, Eq. (9), we have $D^s = D_0$ at all volume fractions.

The systematic force autocorrelation function can be used to obtain $D(t)$ [14],

$$\underline{r}(t) = \underline{r}(0) + (m\xi)^{-1} \int_0^t dt'(\underline{F}(t') + \underline{R}(t')), \tag{15}$$

therefore,

$$\Delta \underline{r}(t)^2 = (m\xi)^{-2} \int_0^t dt'(\underline{F}(t') + \underline{R}(t')) \int_0^t dt''(\underline{F}(t'') + \underline{R}(t'')), \tag{16}$$

which leads to

$$D(t) = \Delta \underline{r}(t)^2/6t = D_0 - \frac{1}{3(m\xi)^2} \int_0^t dt' \langle \underline{F}(0)\underline{F}(t') \rangle, \tag{17}$$

as $\langle \underline{F}\underline{R} \rangle = 0$ and $\langle \underline{R}(t)\underline{R}(t) \rangle = 6mk_B T\xi\delta(t)$. We use both Eq. (10) and Eq. (17) in these calculations and show them to be numerically equivalent for the small N and finite simulation times.

2.3 *Simulation details*

We use Eq. (9) to evolve the particle positions. A feature of this algorithm is that as it is based at the position level, we cannot reproduce the deterministic dynamics valid for $t \ll \tau_B$ of Eq. (13) by taking a very small time step, for example. There is no path to deterministic dynamics therefore. The colloidal particles in our simulations interacted through a soft-sphere interaction,

$$\phi(r) = \varepsilon(\sigma/r)^{36}, \tag{18}$$

where, σ, is the equivalent hard-core diameter of the colloid molecule and, r, is the centre-to-centre separation between the two model particles. The value of the energy parameter ε was set to $\varepsilon = k_B T$ in this study. This interaction could be said to represent a stabilised colloidal particle. The interaction is sufficiently hard to represent a hard-sphere for many purposes, without being too hard which could cause numerical problems in the continuous potential particle update algorithm. This algorithm and hard-core potential has recently been applied to investigate the rheology of colloidal suspensions, including stable suspensions [23], and flocculated suspensions (electro-rheological fluids and depletion flocs) [25, 26]. To be specific and the consistent with our previous work we define the characteristic structural relaxation time, τ_r, to be the time it takes a colloidal particle at infinite dilution to diffuse a distance equal to its radius $a = \sigma/2$,

$$\tau_r = 3\pi\sigma^3\eta_s/4k_B T, \tag{19}$$

or $\tau_r = a^2/D_0$. The quoted thermodynamic quantities and internal programming units are in terms of particle-oriented quantities, where energy is in units of ε, distance is in units of σ and time is in units of $\sigma(m/\varepsilon)^{1/2}$. The dynamic quantities are made dimensionless by dividing by σ for distance, τ_r for time, and D_0 for self-diffusion coefficient. As the value of ε is the unit of energy then the reduced temperature in the model is $T^* = 1.0$.

The random displacement of the particle per time step by the term $\underline{R}$ in the equations of motion of Eq. (9) requires some consideration. The random displacement in the x-direction is related to the infinite-dilution self-diffusion coefficient, D_0, by

$$\langle \delta_x^2 \rangle = 2hD_0, \tag{20}$$

and this was used to determine the time step, h. We first select a desired root mean square displacement for each cartesian component, δ_m, which is an input parameter of the computer program. This parameter is chosen to be small enough to prevent catastrophic overlap of particles and unrealistically large interaction forces, and yet large enough so that a sufficient region of phase space is explored without distorting the statistical averages. Equating $\langle \delta_x^2 \rangle$ (Eq. (20)) to δ_m^2 gives

$$h = \delta_m^2/2D_0, \tag{21}$$

so that the time step is determined by δ_m. A problem with *BD* is that unlike *MD* there is no conserved quantity that can be used to check the stability of the time stepping algorithm. In microcanonical molecular dynamics, for example, the total energy should be constant and independent of time step. Therefore another procedure must be chosen for *BD* to test the adequacy of the implementation of the position update algorithm. The two parameters that can be varied in the computer program are τ_B^* and h^*. We carried out a series of simulations varying both of these parameters. There is a limit to how large τ_B can be because $h/\tau_B = \delta_m^2/2\tau_B^2 k_B T$ and it is necessary for $h/\tau_B \gg 1$ for Eq. (9) to be valid, that is, without needing to include particle momentum in the algorithm. In particle reduced units, provided $h/\tau_B \gg 1$, it does not matter how small τ_B is, nor does it influence the efficiency of travelling through phase space as the key parameter for this, τ_r/h, is independent of the value of τ_B. Several values of τ_B^* were used 0.316×10^{-4}, 0.316×10^{-3} and 0.316×10^{-2} which gives $h/\tau_B = 4.06, 405.6$ and 40558.0 respectively for $\delta_m = 0.009$. The ratio $\tau_r/h = m\sigma^2/2\delta_m^2$ was equal to 6172 in each case. For simulations of duration $t/\tau_r = 16.2$ we found that the thermodynamic and transport coefficients were statistically indistinguishable for the $\phi = 0.472$ state point; $D^L/D_0 = 0.13 \pm 0.01$ and $U/N = 0.886 \pm 0.001$, for example. Similarly using 0.316×10^{-3} and choosing $\delta_m = 0.006$ to 0.009 we found no statistically significant variation. The value of the time step $h^*\tau_B^* < 10^{-4}$ is comparable to the values chosen by other workers [32, 33]. These other authors carried out preliminary *MC* simulations to establish the correct structural and thermodynamic values for the system. The *BD* time step was optimised on the basis of this data. In reduced units, typical values for τ_B, τ_r and h are 0.3×10^{-3}, 791 and 0.13 respectively, for $\delta_x = 0.009$. (These parameters are determined at infinite dilution, and therefore as applied in the computer program are independent of volume fraction.) The computations were conducted using a range of numbers of particles, $N = 108, 256$ and 500 particles, for typically 8×10^5 time steps, using a neighbourhood table list to speed up the search for interacting particles. The simulation cell was cubic and periodically repeated in the three cartesian directions. Interactions were truncated for $r_{ij} > 1.3\sigma$ because of the rapidly decaying nature of the pair potential interactions. In order to make comparisons with the equivalent atomic fluid, molecular dynamics *MD* simulations at $T^* = 1.0$ were carried out using a procedure described elsewhere [35]. The particles were thermostatted at the same temperature as those in the *BD* simulations. The simulations were carried out over many structural relaxation times for the colloidal model systems and also for equivalent times, in terms of particle displacements, for the atomic systems.

The method for calculating the time correlation functions and mean square displacements is essentially that described elsewhere [22], however, the normal procedure of starting a time origin at each time step had to be modified to allow for the extremely slow decay of the autocorrelation function and approach of the m.s.d. to the D^L limit. The time correlation functions have to extend for *ca.* 20,000 time steps for solids volume fractions in excess of *ca.* 0.40. In order to reduce the computer memory requirements, the correlation function was constructed in a piece-wise fashion from three separate correlation functions with time origins started every (and with a resolution of) 1, 10 and 100 time steps. These three correlation functions extended for progressively longer in time, and non-overlapping sections were merged for the purpose of subsequent analysis and presentation. The number of entries in the histogram used to calculate the time

correlation function decreases as time increases. Nevertheless the statistics are reasonable for the ~ 800,000 time steps covered for each production simulation.

3 RESULTS AND DISCUSSION

To appreciate the effects of density on the compaction of an increasingly dense suspension we show in Figure 1 the pair radial distribution function, $g(r)$ as a function of volume fraction for the brownian dynamics states. At $\phi = 0.150$ there is essentially only first peak in $g(r)$, with no well-defined second coordination shell. As density increases, a second and third coordination shell progressively develops in intensity. The first peak becomes sharper, reflecting a reduction in free volume as the system approaches maximum packing and the first coordination shell is forced to become more tightly packed. We considered solids volume fractions between $\phi = 0.075$ and $\phi = 0.527$ defined as $\phi = \pi N\sigma^3/6V$ using the potential σ as a nominal equivalent hard sphere. In fact, this is a reasonable approximation, as can be seen in Figure 1, which indicates very little interparticle penetration for $r < \sigma$. The difference in the $g(r)$ in Figure 1 from comparable state hard-sphere examples is that no penetration for $r < \sigma$ can take place in the hard-sphere case. The hard-sphere $g(r)$ also has a cusped shape as $r \to \sigma$. The soft-potential used here has some penetration for $r < \sigma$ but also has a peak at

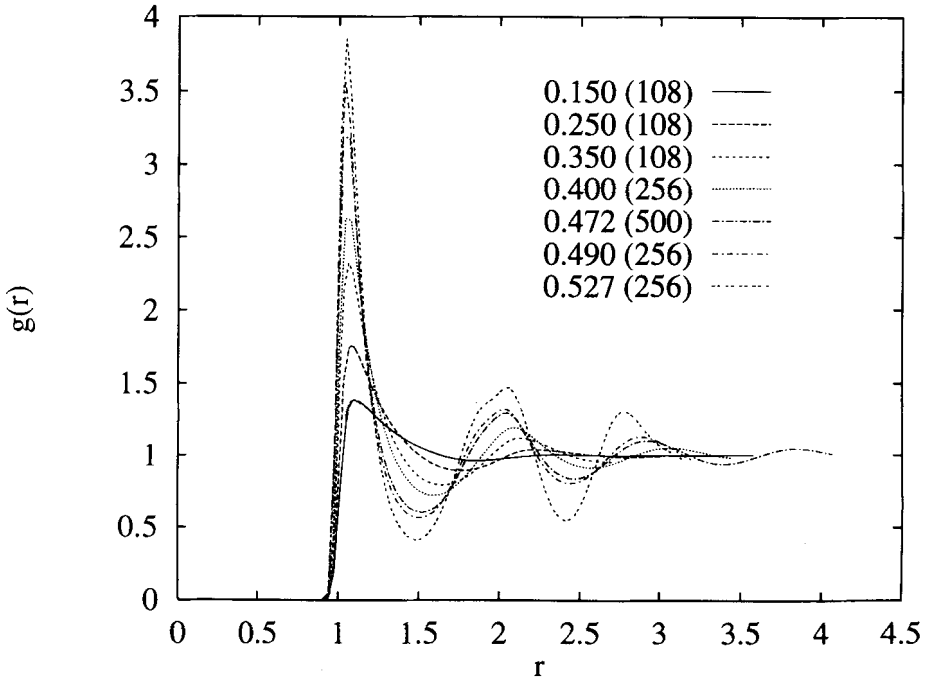

Figure 1 The pair radial distribution function of the *BD* model colloidal liquids. Key: The volume fraction and number of particles in the simulation in brackets are given on the figure.

$r > \sigma$. Therefore, in some sense, σ in the inverse power potential can be said to be a reasonable choice for the equivalent hard-sphere diameter.

The correction to σ to an equivalent hard-sphere diameter depends on the criterion used for matching the physical properties but the multiplicative factor is less than $\sim(1 + n/2)$, where n is the potential exponent, so the potential, $n = 36$ is seen to be equivalent to a hard sphere for the present purposes. In the experimental colloidal systems, correlations to the core diameter, σ_c, due to a soft-repulsive outer shell are for charge stabilised systems $\sim(1 + 2/\kappa\sigma_c)$ where $1/\kappa$ is the double layer thickness, and for sterically stabilised particles, $\sim(1 + 2\Delta/\sigma_c)$ where Δ is the assumed thickness of the stabilising layer. In the colloidal, there are, in these cases, two quite distinct chemical regions composing the "effective" particle, which makes a correction to the nominal volume fraction more necessary than in the case of these model particles. As a guide to the underlying phase diagram, the simulation state $\phi = 0.472$ is close to the maximum equilibrium fluid density of the hard-sphere fluid ($\phi = 0.498$). States above this density show an increasingly pronounced system size and time dependence, reflecting the divergence in structural correlation lengths and times associated with this part of the phase diagram.

In Figure 2, we show the coordination number, $n(r)$,

$$n(r) = 4\pi\rho \int_0^r r^2 dr g(r), \tag{22}$$

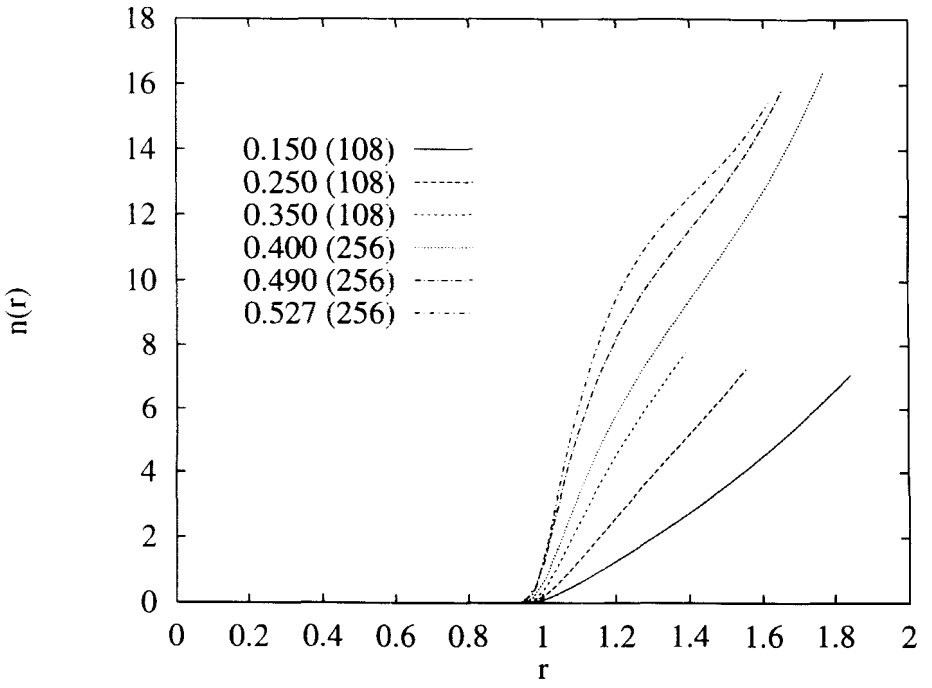

Figure 2 The coordination number in the first coordination shell of the states of Figure 1.

which is the average number of particles in radius r around a particle. We observe a change in functional form of $n(r)$ for $r \to \sigma$, evolving from a $n(r) \sim r^{\alpha}$ where $\alpha < 1$ to $\alpha > 1$ as $\phi > 0.350$. At $\phi = 0.400$ there is less than one neighbouring particle at $r = \sigma$ which then grows to three neighbours at $r = 1.1\sigma$. This rapid increase in average coordination number with r becomes more pronounced as volume fraction increases. In Figure 3 the $g(r)$ for, $\phi = 0.472$, brownian dynamics and molecular dynamics states are compared. They are indistinguishable indicating that the *BD* algorithm is simulating a canonical ensemble to a good approximation. At, $\phi = 0.527$, the system is in the solid-fluid two phase part of the phase diagram. In Figure 4, we compare the $g(r)$ for an *MD* and *BD* state at this volume fraction. The *BD* state manifests a $g(r)$ typical of a liquid (with a some evidence of undercooling evidenced by the shoulder to the second peak), whereas the *MD* state has clearly at least partly nucleated into a microcrystallite, evident in the peak at $r = 1.6\sigma$. The *BD* state at $\phi = 0.527$ is close to the compression glass-transition of a simple liquid, which occurs at $\phi \approx 0.55$ [34]. However, there is no significant evidence of a glassy structure, which would be apparent in a split second peak in the pair radial distribution function. It has been argued that the current *BD* algorithm is incapable of producing a glass because the presence of the Brownian forces ensures that the particles are never at rest [33]. The random force term is decoupled from the other forces and this term keeps the particles in constant motion. In contrast, in *MD*, structurally arrested states are more readily produced, demonstrated by the partly nucleated sample shown in Figure 4.

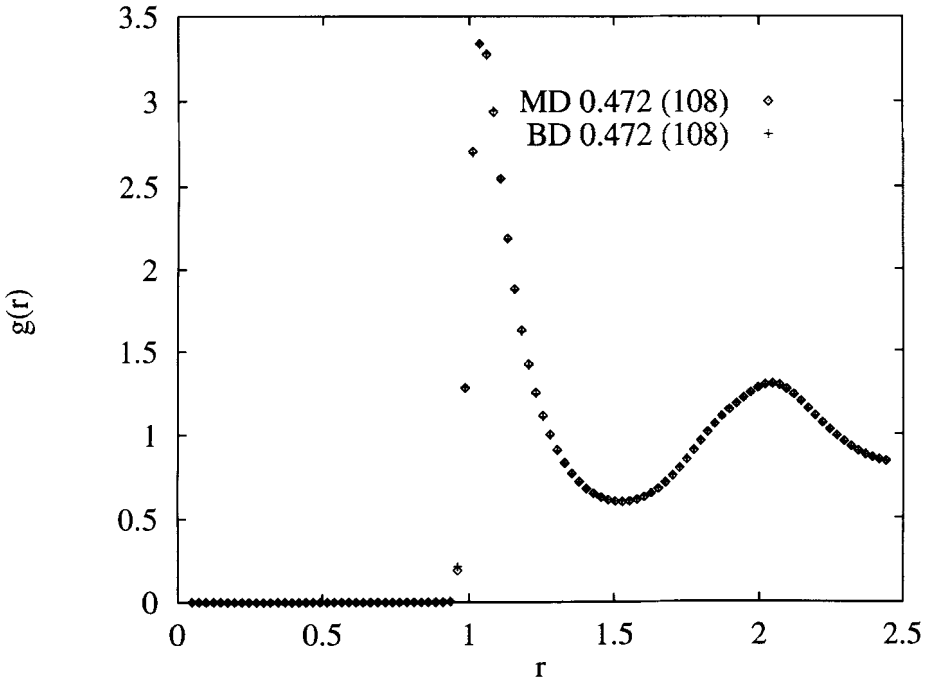

Figure 3 The pair radial distribution function of a *BD* and *MD* simulation at $\phi = 0.472$ with $N = 108$. Key: *MD*, diamonds, and *BD* crosses.

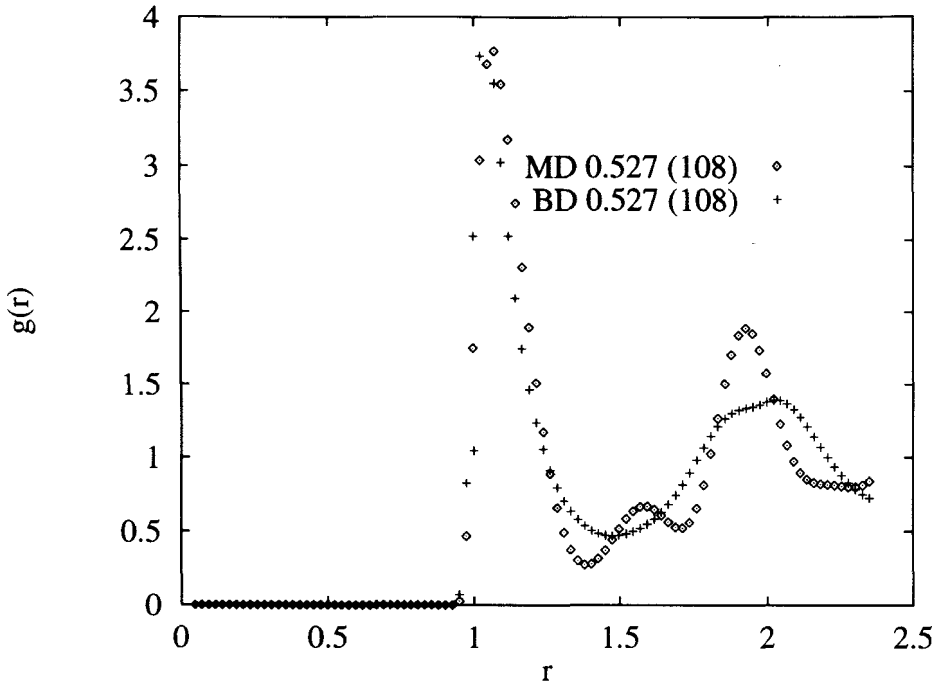

Figure 4 As for Figure 3, except $\phi = 0.527$.

The thermodynamic properties of the *BD* and *MD* systems are compared in Tables 1 and 2, respectively. These tables also give details specific to each simulation carried out. The average potential energy per particle $u = U/N$ is tabulated,

$$\langle u \rangle = \frac{1}{2N} \sum_{i=1}^{N} \sum_{i \neq j} \langle \phi_{ij}(r_{ij}) \rangle. \tag{23}$$

Table 1 Details of the *BD* simulations. Key: The length of the simulation over which averages were collected is t_{sim}.

N	ϕ	t_{sim}/τ_r	U^*/N	$\langle F_x^{*2} \rangle$	D^L/D_0
108	0.075	455	0.03217	27.98	0.880
108	0.115	143	0.05627	48.97	0.799
108	0.150	444	0.08185	71.35	0.749
108	0.250	113	0.1892	166.31	0.581
108	0.350	63	0.3893	346.26	0.402
256	0.400	330	0.5443	485.66	0.291
108	0.427	397	0.6572	590.12	0.253
108	0.472	153	0.8939	811.73	0.154
256	0.472	151	0.8945	811.77	0.150
500	0.472	217	0.9016	819.08	0.157
256	0.490	182	1.0169	927.44	0.124
108	0.500	122	1.0763	984.04	0.110
108	0.527	133	1.0579	955.63	0.0471
256	0.527	113	1.1293	1026.03	0.0293

Table 2 Details of the *MD* simulations using the same particle potential as for the *BD* simulations; otherwise as for Table 1. The simulations were carried out isokinetically at $T^* = 1$. The self-diffusion coefficients using the Erpenbeck (Eq. (3)), Dymond (Eq. (6)) and Speedy formulae (Eq. (2)) are denoted by ERP, DYM and SPD, respectively.

N	ϕ	t^*_{sim}	U^*/N	$\langle F^{*2}_a \rangle$	D^*_{MD}	D^*_{ERP}	D^*_{DYM}	D^*_{SPD}
108	0.150	8020	0.0807	67.41	0.568	0.600	0.676	0.559
108	0.250	5340	0.1882	158.03	0.260	0.295	0.300	0.261
108	0.350	2450	0.3850	325.29	0.107	0.142	0.139	0.124
108	0.400	3000	0.5422	460.04	0.0698	0.0900	0.0888	0.0788
108	0.427	4500	0.6518	554.26	0.0575	0.0671	0.0666	0.0587
108	0.472	19000	0.8814	753.08	0.0289	0.0362	0.0351	0.0315
108	0.527	30000	0.8977	754.37	0.0 (cryst.)	–	–	–

One useful feature of the inverse power, r^{-n}, potentials considered here is that the interaction component of all the equilibrium thermodynamic and mechanical properties are proportional to u. In addition, this functional form has useful scaling behaviour which collapses the phase diagram onto a single ρ, T curve [36]. For example, the potential interaction (osmotic) pressure of the particles in both the *MD* and *BD* states is given by,

$$P = n\rho\langle u \rangle/3. \tag{24}$$

potential, $n = 36$ is in practice very close to the hard-sphere limit. The values for u of the corresponding *BD* and *MD* systems agree within statistical uncertainties, adding to the evidence that both algorithms generate the same distributions in coordinate phase space. Tables 1 and 2 show that there is some N-dependence $\phi > 0.472$ (*BD*) and an increasing difference between *BD* and *MD*. The time step variation study discussed in the Simulation Details section proves that this is not due to the size of the time step being too large. Rather, the observed variation in $\langle u \rangle$ with N is to be expected as these states are close to or within the fluid–solid coexistence part of the phase diagram. The systems become less frustrated with increasing N, allowing closer particle approach on average and therefore an increase in $\langle u \rangle$.

The dynamical behaviour of the two models are quite distinct. In Figure 5, we present the velocity auto-correlattion functions, $C_v(t)$ normalised so that $C_v(0) = 1$, i.e.,

$$C_v(t) = \frac{\langle \underline{\dot{r}}(0) \cdot \underline{\dot{r}}(t) \rangle}{\langle \underline{\dot{r}}^2(0) \rangle}. \tag{25}$$

Examples of the $C_v(t)$ for the atomic fluids at a range of volume fractions are presented in Figure 5. They show a slow monotonic decay at low volume fractions reflecting the weakness of interactions with other particles. At high volume fractions, a negative region appears at intermediate times indicating some "back-scattering" of the particles from their surrounding cages and a much stronger interaction with neighbouring particles. The derived time dependent self-diffusion coefficient is given by,

$$D(t) = \langle \Delta r^2(t) \rangle/6t = \int_0^t dt' \langle \underline{\dot{r}}(0) \cdot \underline{\dot{r}}(t) \rangle (1 - t'/t). \tag{26}$$

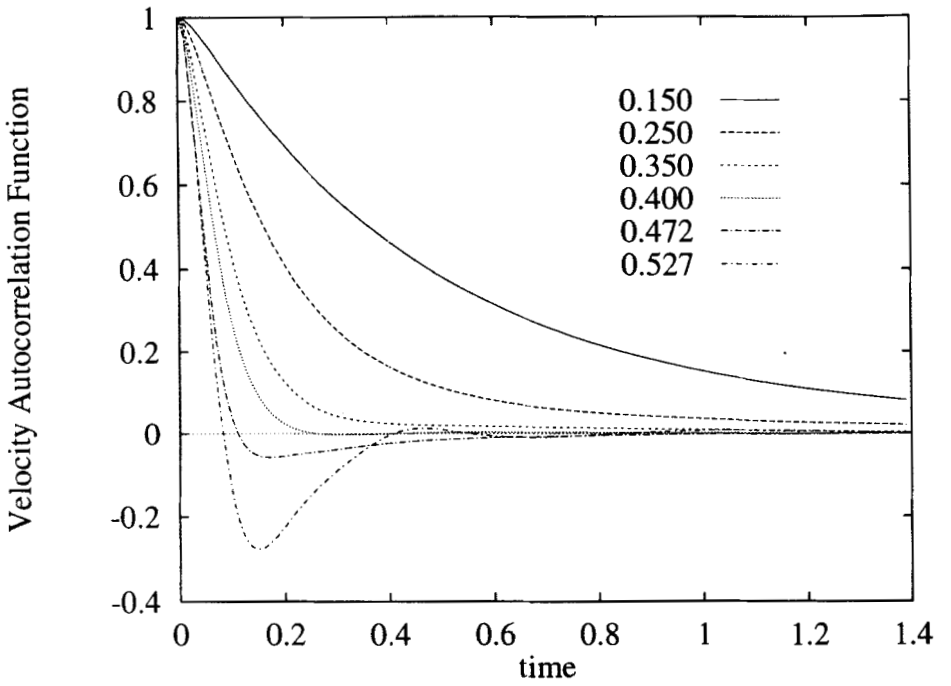

Figure 5 The normalised velocity autocorrelation function of the *MD* states using Eq. (25). The volume fractions are given on the figure.

The $D(t)$ for the data in Figure 5, are given in Figure 6 and the limiting self-diffusion coefficients as $t \to \infty$ are listed in Table 2. Comparisons are made with the Erpenbeck, Dymond and Speedy parametrisations of hard-sphere diffusion coefficients. The hard-sphere D are typically 5–10% larger than the r^{-36} self-diffusion coefficients at the same volume fraction, indicating the effects of the softness of the interaction.

There are no velocities in this *BD* algorithm because $\tau_B \ll h \ll \tau_r$, indicating that the colloidal particle's momentum decays well within the time step, so any "memory" of the particle's velocity is insignificant between successive time steps. In its place, the forces in *BD* assume, in some sense, an equivalent role to that which velocity has in *MD*, in being used to calculate the deviations in the self-diffusion of colloidal particles at finite volume fraction from ideal (i.e., $\phi \to 0$) behaviour (see Eq. (17)). In Figure 7, the normalised $C_F(t)$ calculated as follows,

$$C_F(t) = \frac{\langle \underline{F}(0) \cdot \underline{F}(t) \rangle}{\langle F^2(0) \rangle}, \tag{27}$$

are shown for the atomic fluids. We note that, for the *MD* systems, the $C_F(t)$ show a more pronounced negative region (evident at all volume fractions). The depth of the minimum increases with density and its position moves in to shorter times, which is consistent with the picture that the particle interacts more strongly with its cage of neighbours as number density increases. In Figure 8, the corresponding $C_F(t)$ for the

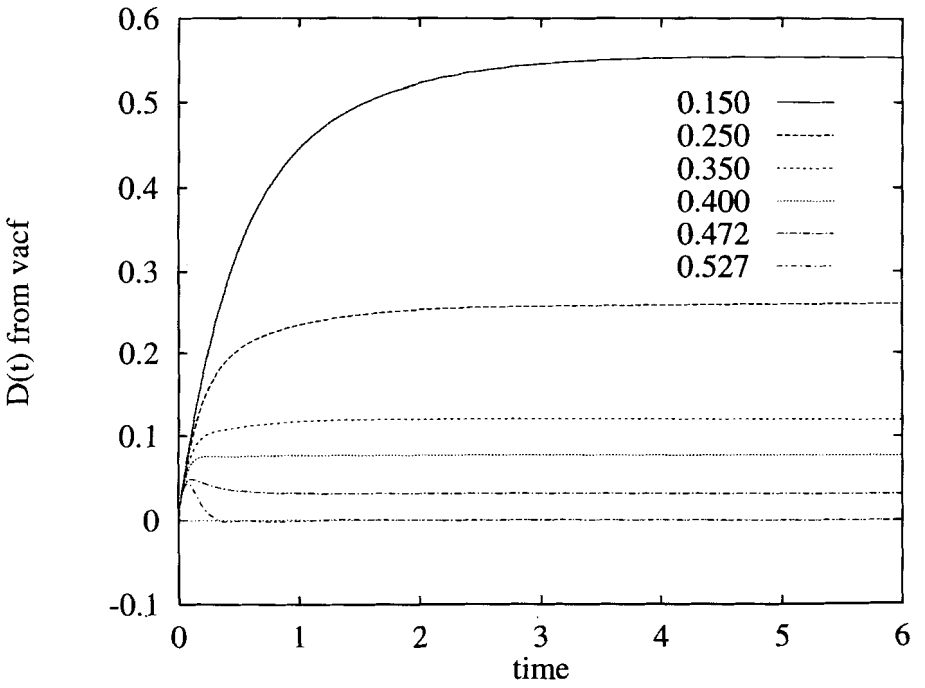

Figure 6 The $D(t)$ using Eq. (26) applied to the velocity autocorrelation functions of Figure 5. The volume fractions are given on the figure.

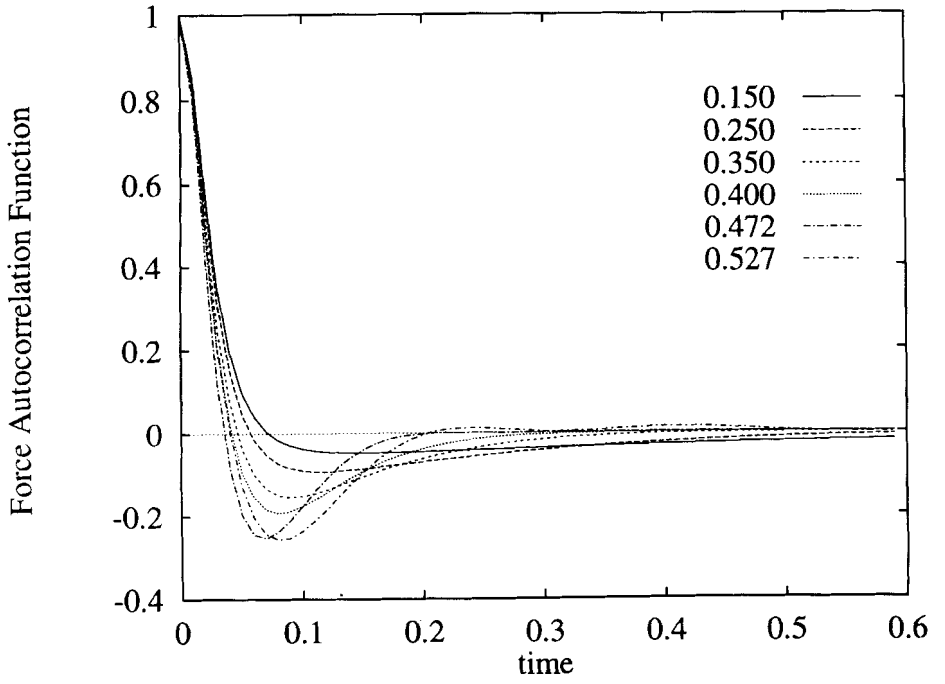

Figure 7 The normalised force autocorrelation function of the *MD* states using Eq. (27). The volume fractions are given on the figure.

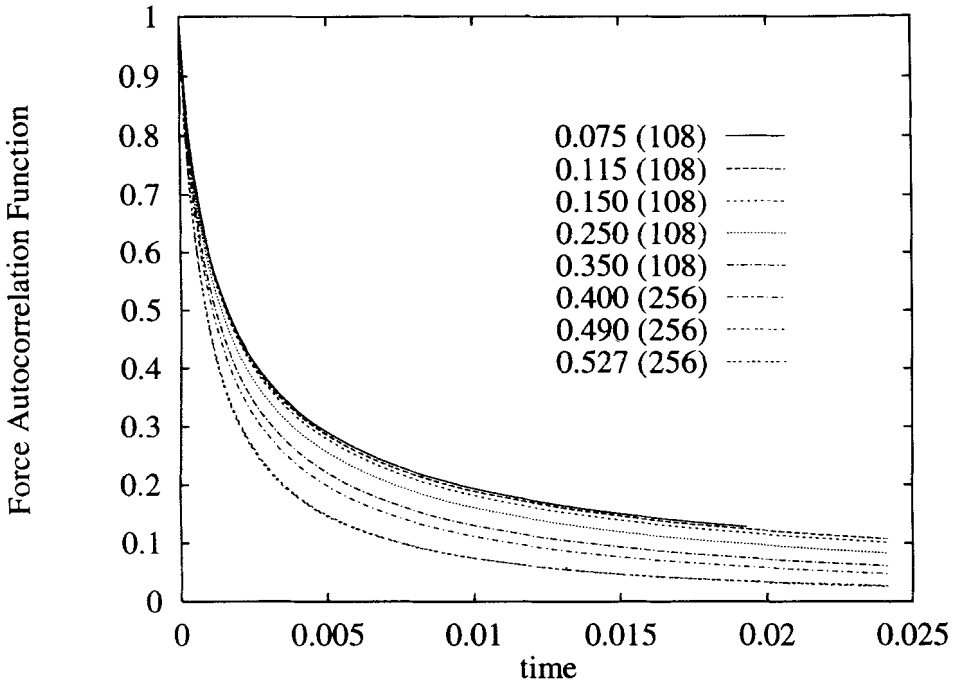

Figure 8 As for Figure 7, except that the *BD* method was used.

brownian systems are shown. They are dramatically different from those of the corresponding atomic fluids, showing no evidence of collision recoil but rather that of the damped dynamics of Langevin *BD* in the $h/\tau_B \to \infty$ limit. The $C_F(t)$ are intregated using Eq. (17) to obtain $D(t)/D_0$. The force autocorrelation function route to the diffusion coefficient of (17) agrees well with the local-slope of the mean square displacement method of Eq. (10), as revealed in Figure 9 for a dense $\phi = 0.490$ *BD* state. The dependence of $D(t)/D_0$ on solids fraction using Eq. (10) is given in Figure 10. To be confident that $D(t)/D_0$ has reached the $t \to \infty$ limit it is necessary to follow the mean square displacements and force autocorrelation function out in time at least $3\tau_r$. As volume fraction increases, the ratio, $D(t)/D_0$, decreases, indicating a reduced mobility of the particles at long times. The $t \to \infty$ limiting values of $D(t)/D_0$ are given in Table 1. We note that although the diffusion coefficients in particle orientated units are quite different for *MD* and *BD*, typically $0.03 - 0.6$ and 3×10^{-4}, respectively, the time steps are much larger in the case of *BD*, so typical displacements per time step are comparable for the two techniques.

In a model without many body-hydrodynamics it is expected that the self-diffusion coefficient as $t \to 0$ will equal D_0 [30], which is what we observe at all densities (see Figure 10).

The first three D^L/D_0 in Table 1, for $\phi = 0.075, 0.115$ and $\phi = 0.150$ fit well to Eq. (1) with the coefficient $a = 1.7 \pm 0.1$ close to the predictions of several effective medium theories without rigorous many-body hydrodynamics, which give $a = 1.8 \pm 0.1$ [6]. The data in Table 1 is compared with some literature experiment and simulation values

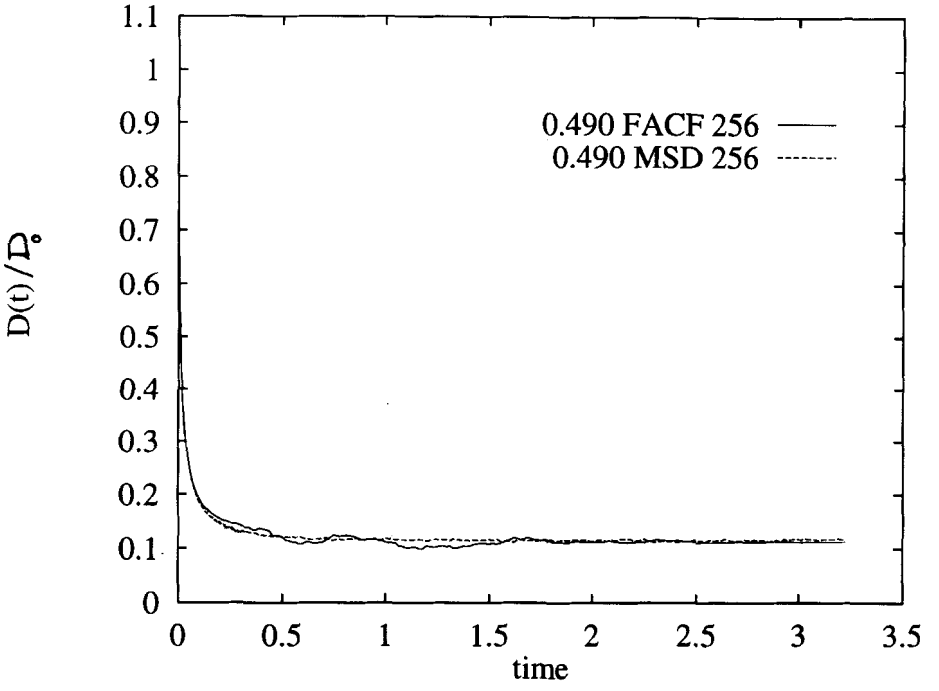

Figure 9 A comparison between the mean square displacement (Eq. (10)) and force autocorrelation function Eq. (17) routes to $D(t)/D_0$ for a $\phi = 0.490$ *BD* state and $N = 256$.

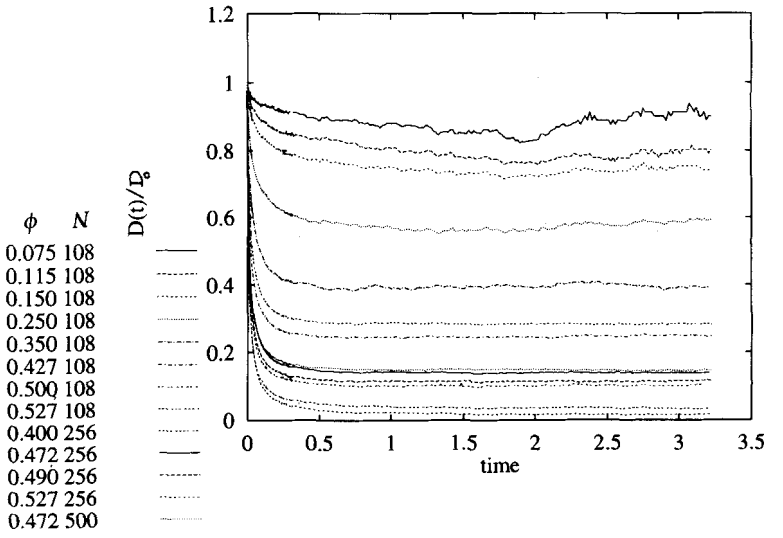

Figure 10 The $D(t)/D_0$ using Eq. (10) applied to the *BD* particle mean-square displacements.

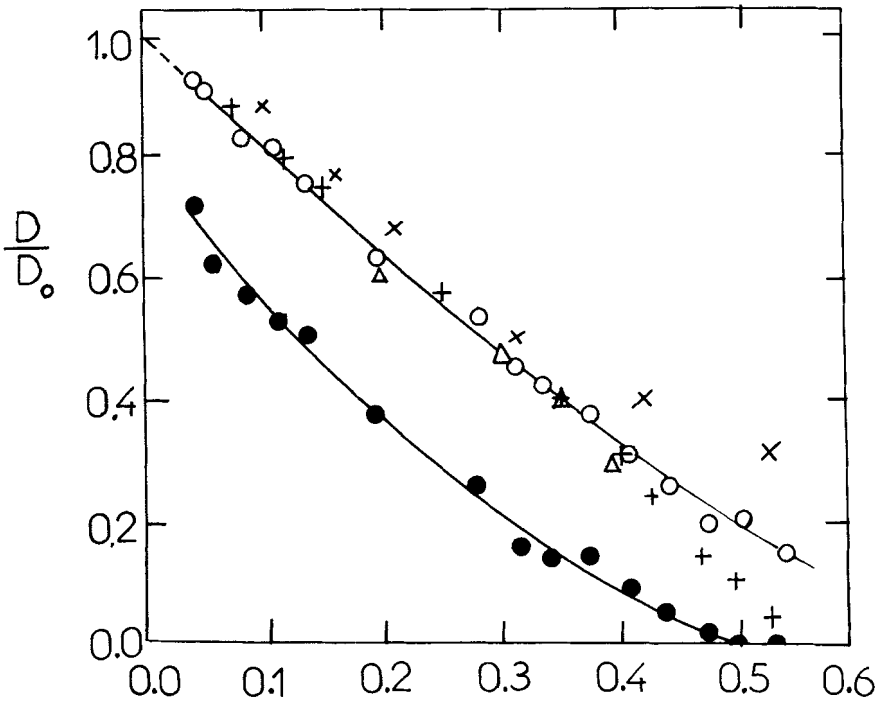

Figure 11 The $D(t)/D_0$ of experimental and simulation. Key: Experiment: [4], PVA stabilised by PHS($\sigma = 0.18\,\mu$m), Open circles, D^S/D_0; filled circles, D^L/D_0; triangles, polystyrene spheres ($\sigma = 0.41\,\mu$m), D^S/D_0 [2]; Simulation: +, this work, × [38].

in Figure 11. Experiments using photon correlation spectroscopy [2, 5] have shown that the ratio, D^S/D_0, decreases essentially linearly with volume fraction. Interestingly the ratio is non-zero (~ 0.17) at the melting volume fraction of 0.54, whereas the D^L/D_0 and the hard-sphere atomic fluids have an essentially zero value for the self-diffusion coefficient at this volume fraction (given by Eq. (2), Eq. (3) and Eq. (6)). The experimental D^S/D_0 is still finite at the freezing transition, indicating that at "short-times" there is still a substantial level of local self-diffusion even though gross movement within the lattice or glass has effectively ceased. There have been a number of brownian dynamics simulations of the self-diffusion coefficient with a screened coulomb interaction, that have examined the concentration dependence of the long-time self-diffusion coefficient [37, 38]. They have all apparently used the same algorithm as in this work, without many-body hydrodynamics. A comparison between the experimental and simulation results is given in Figure 11. The simulation data of D^L/D_0 ironically agrees well with the experimental D^S/D_0 up to $\phi = 0.4$. For higher volume fractions the simulation value of D^L/D_0 decreases more rapidly than the experimental D^S/D_0, however instead tending to zero at $\phi \approx 0.54$, as does the experimental D^L/D_0. Similar behaviour is obtained by the calculations of the long-time self-diffusion coefficient made by Lowen and Szamel [38]. It would appear that the simulation model used in this work gives values for D^L/D_0 that are closer to the experimental D^S/D_0 than to the experimental D^L/D_0. The lack of solvent mediated many-body hydrodynamics clearly causes a major difference

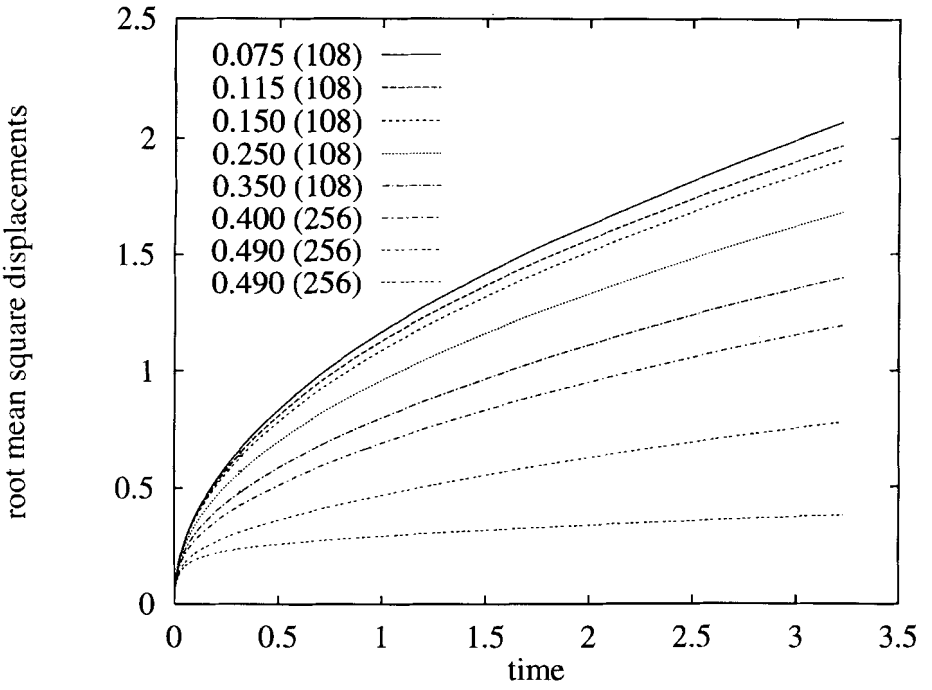

Figure 12 Root mean square displacements of the particles in the *BD* systems as a function of time. The volume fractions and number of particles used are given in the figure, the latter in parentheses.

between the simulation and experimental D^L/D_0. The model gives a D^S/D_0 which is independent of density and equal to unity. In contrast, the experimental D^S/D_0 decreases with volume fraction, presumably because the solvent mediated interactions between the particles cause them to interact even on the "short" time scale (which can be of order a simulation time step).

A notable feature of these simulations is that the model produces a D^L/D_0 which is close to the experimental D^S/D_0 for volume fractions below *ca.* $\phi = 0.4$. The root mean square displacements of the particles are of order σ or greater at the end of the sampling length ($= 3.2\tau_r$) as revealed in Figure 12, so we clearly have achieved displacements at which the surrounding particles have to reorganise for the tagged particle to diffuse further. Yet even at this time we obtain diffusion coefficients which are for $\phi < 0.4$ numerically indistinguishable from D^S, which according to the usual assumption is only valid for displacements $\ll \sigma$. It is as though in the model it is taking the particle several τ_r to interact with other particles in some sense, to the same extent, that real brownian particles do at much shorter times because of the hydrodynamic interactions, which are essentially instantaneous on the particle's time scale. The many-body hydrodynamics acts as a mechanism for rapidly transmitting a force between the particles, so they interact strongly without having to physically collide. The experimental D^L/D_0 are below the D^S/D_0. The coupled hydrodynamics and long distance diffusion of the particles are introducing additional correlations in the particle motion not accounted for by the present model.

For volume fractions in excess of $\phi = 0.4$ the simulation D^L/D_0 fall below the experimental D^S/D_0 and converge on the experimental D^L/D_0 data. Hindered motion due to excluded volume effects at high volume fraction would appear to be reducing (but by no means eradicating) the influence of the brownian motion.

4 CONCLUSIONS

We have made a detailed comparison between the dynamics of a model molecular and colloidal liquid interacting via the same pair potential. Their dynamics have been characterised by force autocorrelation functions and mean square displacements. We have shown that, although the structural and thermodynamic properties of the molecular and colloidal systems with the same interaction potential are distinguishable (as they should be formally), their dynamical behaviour is quite different. The *BD* force autocorrelation functions manifest a damped decay with no negative region. Whereas the *MD* systems show strong backscattering at high volume fraction, evident in a negative region in the force autocorrelation function. The *BD* mean square displacements show no inertial behaviour at short time, in contrast to the *MD* systems. In the colloidal liquids the present simulations have helped establish the important role made by solvent mediated many-body hydrodynamics on colloidal single particle motion *on all diffusive time scales.* For the model colloidal fluid, at all volume fractions, the simulated short-time diffusion coefficient is identical to D_0, that of the experimental colloidal particles at infinite dilution. The simulation long-time diffusion coefficient follows closely the behaviour of the experimental *short*-time diffusion coefficient for volume fractions lower than *ca.* 0.4.

Acknowledgements

Computations were carried out on the CONVEX C3 at the University of London Computer Centre. ACB would like to thank European Community for the award of a research fellowship under the framework, Cooperation in Science and Technology with Central and Eastern European Countries.

References

1. H. N. W. Lekkerkerker and J. K. G. Dhont, *J. Chem. Phys.*, **80**, 5790 (1984).
2. J. Z. Xue, E. Herbolzheimer, M. A. Tutgers, W. B. Russel and P.M. Chaikin, *Phys. Rev. Lett.*, **69**, 1715 (1992).
3. A. van Blaaderen, J. Peetermans, G. Maret and J. K. G. Dhont, *J. Chem. Phys.*, **96**, 4591 (1992).
4. J. W. Goodwin and R. H. Ottewill, *J. Chem. Soc., Faraday Trans.*, **87**, 357 (1991).
5. R. H. Ottewill, *Langmuir*, **5**, 4 (1989).
6. G. T. Evans and C. P. James, *J. Chem. Phys.*, **79**, 5553 (1983).
7. R. Simon, T. Palberg and D. Leiderer, *J. Chem. Phys.*, **99**, 3030 (1993).
8. R. J. Speedy, *Mol. Phys.*, **62**, 509 (1987).
9. J. J. Erpenbeck and W. W. Wood, *Phys. Rev. A*, **43**, 4254 (1991).
10. P. N. Pusey, H. N. W. Lekkerkerker, E. G. D. Cohen and I. M. de Schepper, *Physica A*, **164**, 12 (1990).
11. K. R. Harris, *Mol. Phys.*, **77**, 1153 (1992).
12. R. Buscall, *JCS, Faraday Trans.*, **87**, 1365 (1991)
13. R. Klein, in "Structure and Dynamics of Strongly Interacting Colloids and Supramolecular Aggregates", ed. S.-H. Chen, (1992, Kluwer Academic Publishers) p. 39.
14. T. Akesson and B. Jonsson, *Mol. Phys.*, **54**, 369 (1985).
15. P. Mazur and W. van Saarlos, *Physica*, **115A**, 21 (1982).

16. W. van Megen, I. Snook and P. N. Pusey, *J. Chem. Phys.*, **78**, 931 (1983).
17. C. W. J. Beenakker and P. Mazur, *Physica A*, **120**, 388 (1983).
18. G. Bossis and J. F. Brady, *J. Chem. Phys.*, **91**, 1866 (1989).
19. P. J. Hoogerbrugge and J. M. V. A. Koelman, *Europh. Lett.*, **19**, 155 (1992).
20. D. M. Heyes, *J. Non-Newt. Fl. Mech.*, **27**, 47 (1988).
21. B. J. Alder, D. M. Gass and T. E. Wainwright, *J. Chem. Phys.*, **53**, 3813 (1970).
22. D. Fincham and D. M. Heyes, *Recent Advances in Molecular-Dynamics Computer Simulation, Adv. Chem. Phys.*, in "Dynamical Processes in Condensed Matter", ed. M. Evans (J. Wiley & Sons, N.Y., 1985) pp. 493–575.
23. D. M. Heyes and J. R. Melrose, *J. Non-newt Fl. Mech.*, **46**, 1 (1993).
24. R. H. Ottewill and A. R. Rennie, *Int. J. Multiphase Flow*, **16**, 681 (1990).
25. J. R. Melrose and D. M. Heyes, *J. Chem. Phys.*, **98**, 5873 (1993).
26. J. R. Melrose and D. M. Heyes, *J. Coll. & Interface Sci.*, **157**, 227 (1993).
27. J. L. Hildebrande, *Science*, **174**, 490 (1971).
28. J. H. Dymond, *Physica B*, **144**, 267 (1987).
29. K. D. Hammonds and D. M. Heyes, *J. Chem. Faraday Trans.* 2, **84**, 705 (1988).
30. W. Hess and R. Klein, *Adv. in Phys.*, **32**, 173 (1983).
31. D. L. Ermak, *J. Chem. Phys.*, **62**, 4189 (1975).
32. K. J. Gaylor, I. K. Snook, W. van Megen and R. O. Watts, *Chem. Phys.*, **43**, 233 (1979).
33. H. Lowen, J.-P. Hansen and J.-N. Roux, *Phys. Rev. A*, **44**, 1169 (1991).
34. J. H. R. Clarke, *J. Chem. Soc. Farad. II*, **75**, 1371 (1979).
35. D. MacGowan and D. M. Heyes, *Molec. Simul.*, **1**, 277 (1988).
36. W. G. Hoover, S. G. Gray and K. W. Johnson, *J. Chem. Phys.*, **55**, 1128 (1971).
37. N. Yoshida, *Chem. Phys. Lett.*, **102**, 83 (1983).
38. H. Lowen and G. Szamel, *J. Phys.: Condens. Matter*, **5**, 2295 (1993).